Direct Evidence That All Three Histidine Residues Coordinate to Cu(II) in Amyloid-β_{1-16}[†]

Byong-kyu Shin and Sunil Saxena*

Department of Chemistry, University of Pittsburgh, Pittsburgh, Pennsylvania 15260

Received May 29, 2008; Revised Manuscript Received July 10, 2008

ABSTRACT: We provide direct evidence that all three histidine residues in amyloid-β_{1-16} (Aβ_{1-16}) coordinate to Cu(II). In our approach, we generate Aβ_{1-16} analogues, in each of which a selected histidine residue is isotopically enriched with ^{15}N. Pulsed electron spin resonance (ESR) experiments such as electron spin echo envelope modulation (ESEEM) and hyperfine sublevel correlation (HYSCORE) spectroscopy clearly show that all three histidine imidazole rings at positions 6, 13 and 14 in Aβ_{1-16} bind to Cu(II). The method employed here does not require either chemical side chain modification or amino acid residue replacement, each of which is traditionally used to determine whether an amino acid residue in a protein binds to a metal ion. We find that the histidine coordination in the Aβ_{1-16} peptide is independent of the Cu(II)-to-peptide ratio, which is in contrast to the Aβ_{1-40} peptide. The ESR results also suggest tight binding between the histidine residues and the Cu(II) ion, which is likely the reason for the high binding affinity of the Aβ peptide for Cu(II).

Amyloid-β (Aβ)[1] is a naturally occurring peptide with 39−43 amino acid residues. The aggregation of Aβ is deeply associated with the onset of Alzheimer's disease, the most common form of dementia. The intermediates in the aggregation process have been suggested to play a major role in the toxicity of the disease (*1*−*5*). It is believed that transition metal ions such as Cu(II) and Zn(II) stabilize the toxic intermediates by coordinating with the Aβ peptide (*6*−*10*). Also, the in vitro misfolding mechanism of Aβ peptide is found to be governed by the concentration of Cu(II) ions (*11*). The role of Cu(II) ions in Aβ peptide aggregation has, therefore, aroused recent scientific interest.

From a molecular point of view, however, some uncertainty about the Cu(II) coordination site, which constitutes a fundamental determinant of the metal−peptide interaction, still exists. The work performed by Karr et al. suggests that the two main forms, Aβ_{1-40} and Aβ_{1-42}, have essentially the same Cu(II)-binding site as shorter Aβ peptides, Aβ_{1-16} and Aβ_{1-28} (*12*−*14*). They also argue that one of the three histidine residues, presumably His14, is unlikely to be bound to Cu(II) because their continuous wave-electron spin resonance (CW-ESR) data are consistent with 3N1O coordination and one of the nitrogen ligands is located in the N-terminus (*13, 15*). On the other hand, potentiometric titrations performed by Kowalik-Jankowska et al. suggest that two histidine residues, His13 and His14, coordinate to Cu(II) in Aβ_{1-16} and Aβ_{1-28} at a physiological pH (*16*). However, NMR experiments performed with Aβ_{1-28} analogues by Syme et al. indicate that His6, His13, and His14 as well as the N-terminus are the ligands which coordinate to Cu(II) (*17*). Indeed, the Cu(II) coordination of each histidine residue has remained unresolved until lately, as seen in the three different coordination models for Cu(II)−Aβ_{1-42} complexes proposed by Raffa et al. (*18*). In this context, we have sought to find a way to unequivocally determine which histidine residues coordinate to Cu(II).

We have used the approach of Burn et al. to investigate Cu(II)−peptide complexes (*19*−*21*). Using pulsed ESR techniques and ^{15}N-enriched peptides, they successfully identified the Cu(II) coordination site in the prion protein to be a short sequence, HGGGW (*20*). In this article, we assess the Cu(II) coordination of the three histidine residues in the Cu(II)−Aβ_{1-16} complex by pulsed ESR spectroscopy. To observe the interaction between the Cu(II) ion and each histidine residue, we designed three different ^{15}N-labeled Aβ_{1-16} peptide analogues, in each of which only one of the three histidine residues is isotopically enriched with ^{15}N. Pulsed ESR experiments such as electron spin echo envelope modulation (ESEEM) and hyperfine sublevel correlation (HYSCORE) on the ^{15}N-labeled peptide analogues reveal that all three histidine residues, His6, His13, and His14, bind to Cu(II). This approach does not require either amino acid side chain modification or replacement of specific amino acid residue(s), each of which is a traditional way of determining whether an amino acid residue coordinates to a metal ion. Our experiments also indicate very little dependence of Cu(II)−histidine coordination on the molar ratio of Cu(II) to Aβ_{1-16} peptide. This result is contrasted with the case of Aβ_{1-40} (*11*). In addition, we observe a strong hyperfine interaction between the Cu(II) ion and the remote nitrogen of histidine imidazole by analysis of HYSCORE spectra. The strong interaction suggests a tight binding of histidine to

[†] This work was supported by a National Science Foundation CAREER grant (MCB 0346898).

* To whom correspondence should be addressed. Phone: (412) 624-8680. Fax: (412) 624-8611. E-mail: sksaxena@pitt.edu.

[1] Abbreviations: Aβ, amyloid-β; ESR, electron spin resonance; ESEEM, electron spin echo envelope modulation; HYSCORE, hyperfine sublevel correlation; CW, continuous wave; NEM, *N*-ethylmorpholine; NQI, nuclear quadrupole interaction.

10.1021/bi801014x CCC: $40.75
Published on Web 08/09/2008

Cu(II), which is likely the reason for the high affinity of the Aβ peptide for Cu(II) (*17, 22*).

EXPERIMENTAL PROCEDURES

Peptide Synthesis and Cu(II)−Peptide Complex Preparation. Three different analogues of the Aβ_{1-16} peptide, DAEFRHDSGYEVHHQK, with an ^{15}N-labeled histidine residue at either position 6 (Aβ_{1-16}H6[^{15}N]), position 13 (Aβ_{1-16}H13[^{15}N]), or position 14 (Aβ_{1-16}H14[^{15}N]) were synthesized at the Peptide Synthesis Facility of the University of Pittsburgh. Isotopically enriched [G-^{15}N]-N_α-Fmoc-N_τ-trityl-L-histidine, in which all nitrogen atoms are enriched with ^{15}N, was purchased from Cambridge Isotope Laboratory (Andover, MA). Each of the analogues was characterized by high-performance liquid chromatography and mass spectrometry. Nonlabeled Aβ_{1-16} peptide was purchased from rPeptide (Bogart, GA).

Isotopically enriched [^{63}Cu]Cl_2 was purchased from Cambridge Isotope Laboratory. A 100 mM *N*-ethylmorpholine (NEM) buffer with a pH of 7.4 was prepared by mixing NEM and hydrochloric acid in 50% glycerol. Then, 2.5 mM solutions of Aβ_{1-16}, Aβ_{1-16}H6[^{15}N], Aβ_{1-16}H13[^{15}N], and Aβ_{1-16}H14[^{15}N] were prepared in the 100 mM NEM buffer. Separately, a 10 mM Cu(II) stock solution was prepared in the same buffer. For the nonlabeled Aβ_{1-16} peptide and each of the three ^{15}N-labeled analogues, 1:1 and 0.25:1 Cu(II)-to-peptide molar ratio mixtures were prepared with a final concentration of 1.25 mM in the peptide. For the nonlabeled Aβ_{1-16} peptide, a 4:1 mixture was additionally prepared.

ESR Spectroscopy. For ESR experiments, 200 μL of each Cu(II)−peptide mixture solution was transferred into a quartz tube with an inner diameter of 3 mm. ESR experiments were carried out on a Bruker ElexSys E580 FT/CW X-band spectrometer equipped with a Bruker ER 4118X-MD5 dielectric ring resonator. The temperature was adjusted with an Oxford ITC503 temperature controller and an Oxford CF935 dynamic continuous flow cryostat.

Three-pulse ESEEM experiments were performed on all of the sample solutions at 20 K with a stimulated echo pulse sequence of $\pi/2-\tau-\pi/2-T-\pi/2-\tau-$echo. The first pulse separation, τ, was set at 200 ns, and the second pulse separation, T, was varied from 400 ns with a step size of 16 ns for a total of 1024 points. The pulse length was 16 ns for $\pi/2$, and the magnetic field strength was fixed at approximately 3360 G, where the echo intensity was a maximum. In addition, a four-step phase cycle was employed to eliminate unwanted signals (*23, 24*). The maximum intensity of the data was normalized to 1, and the baseline decay was subtracted before Fourier transformation.

Four-pulse HYSCORE experiments were performed on all of the 1:1 mixture solutions at 20 K with a pulse sequence of $\pi/2-\tau-\pi/2-t_1-\pi-t_2-\pi/2-\tau-$echo. The first pulse separation, τ, was set at 200 ns, and both of the second pulse separation, t_1, and the third pulse separation, t_2, were varied from 200 ns with a step size of 16 ns for a total of 256 points. The maximum intensity of the data was normalized to 1, and the baseline decay was subtracted. Then, the data were zero-filled to 1024 points before Fourier transformation. The pulse lengths were 16 and 32 ns for $\pi/2$ and π pulses, respectively, and the magnetic field strength was fixed at approximately 3360 G, where the echo intensity was a maximum. In addition, a four-step phase cycle was employed to eliminate unwanted signals.

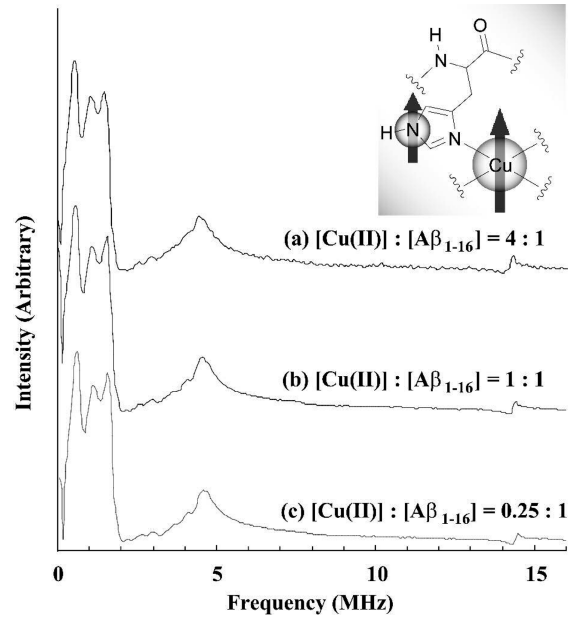

FIGURE 1: ESEEM spectra of nonlabeled Aβ_{1-16} mixed with Cu(II) at different molar ratios. The three sharp peaks (0−2 MHz) and one broad peak (≈4.5 MHz) are unique to the Cu(II) bound to imidazole ring(s). No significant difference in spectra a−c indicates little effect of the Cu(II) level on the binding environment.

RESULTS AND DISCUSSION

All ESR experiments were carried out on the nonlabeled Aβ_{1-16} peptide and three labeled Aβ_{1-16} analogues. Each of the three labeled analogues has one ^{15}N-labeled histidine residue at either His6, His13, or His14. These ^{15}N-labeled peptide analogues are termed Aβ_{1-16}H6[^{15}N], Aβ_{1-16}-H13[^{15}N], and Aβ_{1-16}H14[^{15}N], respectively.

Evidence of Cu(II)−Histidine Coordination in Aβ_{1-16}. Three-pulse ESEEM experiments were performed on the mixtures of Cu(II) and the nonlabeled Aβ_{1-16} with three different Cu(II)-to-peptide ratios of 4:1, 1:1, and 0.25:1. The ESEEM spectra of the three mixtures are illustrated in Figure 1. Each of the spectra has three peaks at or around 0.55, 1.04, and 1.53 MHz. The sum of the lower two frequencies is almost equal to the highest one within the resolution error range of ±0.03 MHz, which indicates that the three peaks are presumably due to the nuclear quadrupole interaction (NQI) (*25*). The three ESEEM frequencies, ν_0, ν_-, and ν_+, for the ^{14}N ($I = 1$) NQI transitions are given by (*25*)

$$\nu_0 = \frac{\eta e^2 qQ}{2h}; \nu_- = \frac{e^2 qQ(3-\eta)}{4h}; \nu_+ = \frac{e^2 qQ(3+\eta)}{4h} \quad (1)$$

where e is the unit charge, q is the z-component of the electric field gradient across the nucleus, Q is the ^{14}N nuclear quadrupole moment, η is the asymmetry parameter, and h is Planck's constant.

With these frequencies in eq 1, the nuclear quadrupole parameters, e^2qQ/h and η, are determined to be 1.71 ± 0.03 MHz and 0.64 ± 0.02, respectively. All of these values, including the three frequencies and the two calculated parameters, are comparable to those for many Cu(II)−imidazole complexes that were determined by McCracken et al. (*26−28*).

Their research has shown that the interaction between the Cu(II) and the remote nitrogen of the coordinated imidazole ring causes three different nuclear quadrupole frequencies. In their experiments, the three frequencies, ν_0, ν_-, and ν_+, range from 0.45 to 0.70 MHz, from 0.70 to 1.10 MHz, and from 1.40 to 1.55 MHz, respectively, and the calculated e^2qQ/h and η values were between 1.44 and 1.73 MHz and between 0.48 and 0.98, respectively (*28*).

In addition, the appearance of the broad peak around 4.5 MHz is due to the ^{14}N double-quantum transition. The theoretical frequency is given by (*29*)

$$\nu_{dq} = 2\sqrt{\left(\nu_I + \frac{A}{2}\right)^2 + \left(\frac{B}{2}\right)^2 + \left(\frac{e^2qQ}{4h}\right)^2(3+\eta^2)} \qquad (2)$$

where ν_{dq} is the double-quantum transition frequency, ν_I is the Larmor frequency of ^{14}N, and A and B are the secular and the pseudosecular part of the hyperfine interaction, respectively. The theoretical value is calculated with the nuclear quadrupole parameters, e^2qQ/h and η, and one of the ^{15}N transition frequencies obtained in HYSCORE experiments (0.41 and 2.63 MHz; see below) on the basis of the fact that ν_I, A, and B in eq 2 are proportional to the g factor of the nucleus. The theoretical value of ν_{dq} is approximately 4.10 ± 0.14 MHz which is comparable to the position of the broad peak.

Each of the spectra in Figure 1 also has a small peak around 14.3 MHz, which is almost the Larmor frequency of ^{1}H at the applied magnetic field. The position indicates that the peak is due to hydrogen atom(s) that weakly interact with the Cu(II), such as those of axially coordinated water or other remote hydrogen atom(s) (*20*).

On the basis of the analysis of the peaks in Figure 1, it is concluded that at least one histidine residue coordinates to Cu(II). Also, the almost unchanged peak positions, shapes, and intensities of the three spectra obtained with different Cu(II)-to-peptide ratios imply that the coordination environment in Aβ_{1-16} is not significantly affected by the Cu(II) level. This finding is in contrast to the Cu(II)−Aβ_{1-40} complex, for which the ESEEM spectrum becomes broad and heterogeneous at greater than equimolar concentrations (*11*). We propose that Aβ_{1-16} has only one Cu(II)-binding site, whereas the larger peptide, Aβ_{1-40}, might have additional binding site(s). Syme et al. have also suggested that two Cu(II)-binding sites are present in Aβ_{1-28} (*17*). Another possibility might be that the binding sites in Aβ_{1-16} and Aβ_{1-40} have different numbers of histidine ligands. In this context, Karr et al. have argued that both His13 and His14 cannot coordinate to Cu(II) in a β-sheet structure in Aβ_{1-40} because the structure would be disrupted by the simultaneous coordination of two adjacent residues (*13*). It is conceivable that the Cu(II) coordination of His13 and His14 may not be restricted in Aβ_{1-16} since it is soluble and highly flexible at a physiological pH.

Direct Proof of the Cu(II) Coordination of the Three Histidine Residues (His6, His13, and His14). The peak positions in Figure 1 are similar to those for the Cu(II)-bound short peptide chain (HGGGW) which was studied by Burns et al.; ν_0, ν_-, and ν_+ are 0.57, 0.90, and 1.47, respectively (*20*). Unlike the short chain HGGGW, however, the Aβ_{1-16} peptide has three histidine residues that may contribute to the ESEEM spectrum. Kosman et al. showed that there may

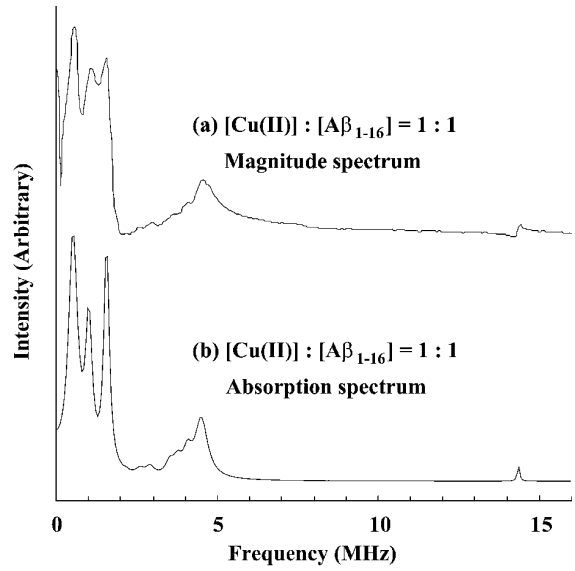

FIGURE 2: Comparison of magnitude and absorption ESEEM spectra of nonlabeled Aβ_{1-16} mixed with an equimolar amount of Cu(II). Compared with the magnitude spectra, the absorption spectra have narrower line widths, which provide clear peak separations in the histidine ESEEM region (0−10 MHz).

be harmonics and combination peaks between 2 and 3.5 MHz if two or more histidine residues are bound to Cu(II) (*30, 31*). Indeed, several additional peaks were clearly observed in spectral simulations that include contributions from two or three remote ^{14}N nuclei (data not shown). The line widths of the magnitude spectra are broad, as shown in Figure 1. To improve the resolution, we obtained the pure absorption spectrum by manipulating the corresponding time domain signals with the algorithm developed by Astashkin et al. (*32*). The pure absorption spectum is presented in Figure 2. Even in the absorption spectrum, the peaks between 2 and 3.5 MHz are not sufficiently resolved to discern harmonics or combination peaks from the baseline.

To make progress, we prepared three different singly labeled Aβ_{1-16} peptide analogues which are labeled with ^{15}N at His6, His13, and His14. Then, a three-pulse ESEEM experiment was performed on the equimolar mixture of Cu(II) and each ^{15}N-labeled analogue. The normalized time domain ESEEM signals of the four Cu(II)−peptide complexes are shown in Figure 3. It is known that the modulation depth in the time domain signal increases with the number of equivalent ESEEM-active nuclei (*33*). Especially, the modulation depth that is much smaller than 1 is almost directly proportional to the number of equivalent nuclei with the same frequency (*33, 34*). Recently, Vogt et al. have determined the number of water molecules coordinated to Mn(II) by comparing modulation depths between experimental ^{2}H ESEEM spectra and simulation (*35*). In our experiments, the modulation depth in the time domain ESEEM signals is related to the number of ^{14}N-enriched histidine residues coordinated to Cu(II). Unlike the ^{14}N NQI and double-quantum transitions, the ^{15}N ($I = {}^1/_2$) single-quantum transition may not meaningfully contribute to the modulation depth of time domain signals or corresponding ESEEM spectra (*36*−*39*). The comparison of the four signals in Figure 3 clearly shows that the nonlabeled complex has a larger modulation depth than the other three, the ^{15}N-labeled

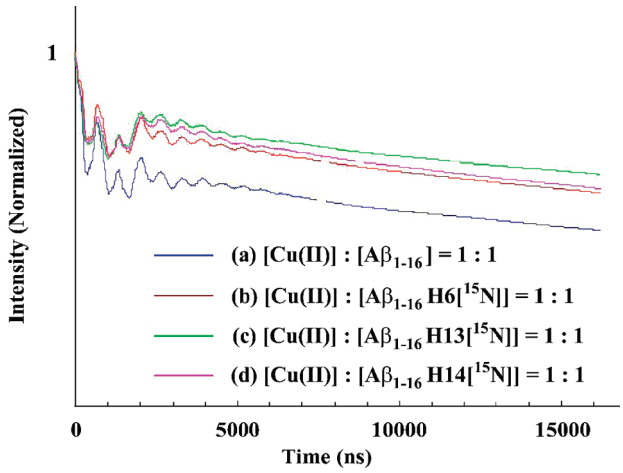

FIGURE 3: Time domain ESEEM signals of nonlabeled Aβ_{1-16} and ^{15}N-labeled analogues mixed with an equimolar amount of Cu(II). The modulation depth of the nonlabeled complex is significantly larger than the others.

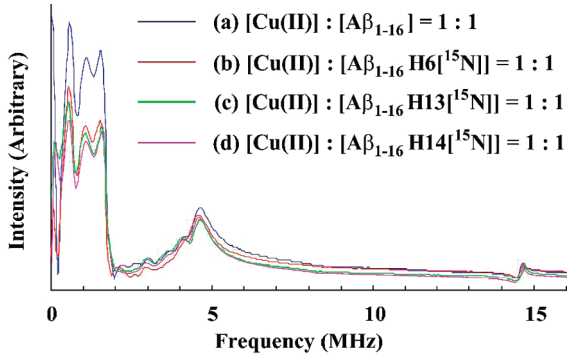

FIGURE 4: ESEEM spectra of nonlabeled Aβ_{1-16} and ^{15}N-labeled analogues mixed with an equimolar amount of Cu(II). The area under the curve for the histidine ESEEM region (0−10 MHz) of the nonlabeled Aβ_{1-16} complex is approximately 1.5 times that of the ^{15}N-labeled Aβ_{1-16} complexes, while the four spectra have similar intensities in the ^{1}H ESEEM region (14−15 MHz).

analogues, which signifies that there are more ESEEM-active ^{14}N nuclei for the Cu(II)−nonlabeled peptide complex.

To unambiguously determine the number of coordinated histidine residues, we also analyzed the integrated intensity in the corresponding ESEEM spectra. Since the integrated intensity of the ESEEM spectra is related to the modulation depth, it should decrease when one histidine residue is labeled with ^{15}N. This expectation is backed by spectral simulations that include contributions from one, two, or three remote ^{14}N nuclei (data not shown). Figure 4 shows the ESEEM spectra of the four Cu(II)−peptide complexes. Compared with the spectrum of the Cu(II)−nonlabeled peptide complex, each of the spectra of the Cu(II)-bound ^{15}N-labeled analogues has considerably lower intensity in the histidine ESEEM region (0−10 MHz). The lower intensity of ^{15}N-labeled analogues in Figure 4 can be attributed to the replacement of an ESEEM-active ^{14}N nucleus with a ^{15}N nucleus as shown in the work of Burns et al. (*20*). As shown in Table 1, the area under the curve for the histidine ESEEM region (0−10 MHz) of the nonlabeled complex is approximately 1.5 times as great as that of the ^{15}N-labeled analogues. On the other hand, the area under the curve for the ^{1}H ESEEM region (14−15 MHz) remains constant within an error range of ±3%. Since any of the ^{15}N-labeled analogues should have one fewer ESEEM-active ^{14}N nucleus, the ratio (1.5:1) is

Table 1: Areas under the Curves of the ESEEM Spectra in Figure 4

	(a) area[a] (0−10 MHz)	(b) area[a] (14−15 MHz)	ratio (a/b)
Cu(II)−Aβ_{1-16}	1.01×10^5	3.37×10^3	30.0
Cu(II)−Aβ_{1-16}H6[^{15}N]	6.82×10^4	3.34×10^3	20.4
Cu(II)−Aβ_{1-16}H13[^{15}N]	6.85×10^4	3.27×10^3	20.9
Cu(II)−Aβ_{1-16}H14[^{15}N]	6.71×10^4	3.41×10^3	19.7

[a] Values are in arbitrary units.

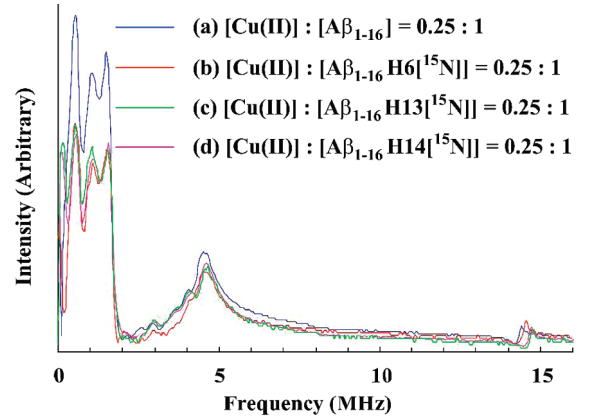

FIGURE 5: ESEEM spectra of nonlabeled Aβ_{1-16} and ^{15}N-labeled analogues mixed with a subequimolar amount of Cu(II). The ratio of Cu(II) to peptide is 0.25:1. The area under the curve for the histidine ESEEM region (0−10 MHz) of the nonlabeled Aβ_{1-16} complex is approximately 1.5 times that of the ^{15}N-labeled Aβ_{1-16} complexes, while the four spectra have similar intensities in the ^{1}H ESEEM region (14−15 MHz).

consistent with three and two contributing ^{14}N nuclei for the nonlabeled Aβ_{1-16} and ^{15}N-labeled analogues, respectively.

Whereas the three ^{14}N NQI peaks between 0 and 3 MHz display a clear difference in intensity between the nonlabeled peptide and the ^{15}N-labeled analogues, the difference in intensity of the ^{14}N double-quantum peak around 4.5 MHz is smaller. The area under the curve for the double-quantum region (3−6 MHz) of the Cu(II)−nonlabeled peptide complex is approximately 1.3 times that of the ^{15}N-labeled analogues. We suspect that the use of magnitude spectra, combined with the broad line width and the low signal-to-noise ratio of the double-quantum peak, partially explains the deviation from the expectation. The intensity of the double-quantum peak is also very sensitive to the separation between the first and second pulses (*39*).

To confirm that the three histidine residues still coordinate to Cu(II) at different Cu(II) levels, we also performed the three-pulse ESEEM experiment on the 0.25:1 mixture of Cu(II) and each ^{15}N-labeled analogue. Figure 5 shows the ESEEM spectra of the subequimolar mixtures of the Cu(II)−nonlabeled Aβ_{1-16} peptide and the Cu(II)−^{15}N-labeled analogue complexes. When compared with the ESEEM spectra of the equimolar mixtures, shown in Figure 4, those of the subequimolar mixtures also reveal a similar difference in intensity between the nonlabeled peptide and the ^{15}N-labeled analogues. The peak positions are nearly identical to those for the ESEEM spectra of the equimolar mixtures, and the intensity in the histidine ESEEM region (0−10 MHz) is significantly higher for the Cu(II)−nonlabeled peptide complex as in the equimolar mixtures. This points out the fact that no histidine residue is substantially preferred over the others as a ligand at a low Cu(II)-to-peptide ratio such as 0.25:1. Therefore, we conclude that the three histidine

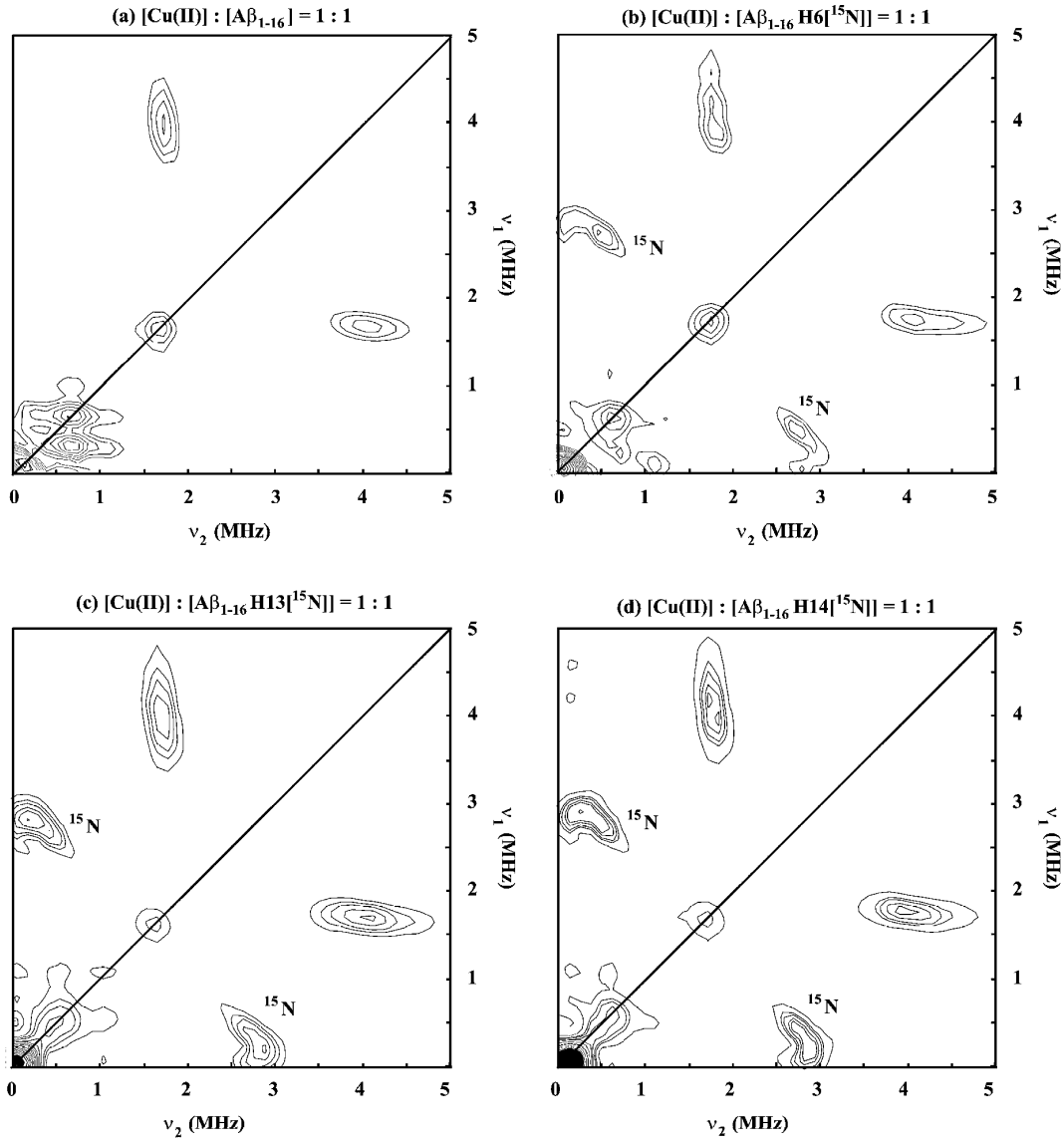

FIGURE 6: HYSCORE spectra of ^{15}N-labeled and nonlabeled Aβ_{1-16} mixed with an equimolar amount of Cu(II). (a) The spectrum of the Cu(II)−nonlabeled peptide complex lacks a cross-peak at or around (0.41 MHz, 2.63 MHz) which appears in the other three spectra (b−d).

residues simultaneously coordinate to Cu(II) at a range of Cu(II)-to-peptide ratios, at least from 0.25:1 to 1:1.

Calculation of Hyperfine Coupling Parameters by Analysis of HYSCORE Spectra. The interaction between each histidine residue and Cu(II) is more evident from HYSCORE experiments. In HYSCORE, the π pulse between the second and third $\pi/2$ pulses creates the correlation between the nuclear coherences of the two different electron spin manifolds (*40*−*42*). Also, the HYSCORE technique helps resolve some lines which are broadened in the ESEEM spectrum (*43*−*45*). To obtain more detailed spectroscopic information about the Cu(II)−Aβ_{1-16} peptide complex, HYSCORE experiments were performed on the equimolar mixture of Cu(II) and each peptide analogue. The HYSCORE spectrum of the Cu(II)−nonlabeled peptide complex shown in Figure 6a contains a cross-peak around (1.5 MHz, 4.0 MHz). This peak appears due to the correlation between the ^{14}N NQI and double-quantum transition for the noncoordinating nitrogen of the histidine imidazole (*20, 28*). While it is also observed in the HYSCORE spectra of the Cu(II)−^{15}N-labeled peptide complexes, a new cross-peak emerges at or around (0.41 MHz, 2.63 MHz) in each of the ^{15}N-labeled analogues. The cross-peak is comparable to the ^{15}N cross-peak observed in the HYSCORE spectrum of the ^{15}N-labeled Cu(II)−HGGGW complex in terms of peak position and contour line shape (*20, 36*). Moreover, the average of the two frequencies, 1.52 MHz, is close to 1.45 MHz, the Larmor frequency of ^{15}N corresponding to a magnetic field of 3360 G at which our ESEEM and HYSCORE experiments were carried out. Thus, the cross-peak is due to the correlation between the ^{15}N transitions in different electron spin manifolds. The two frequencies, ν_α and ν_β, are given by (*46*−*48*)

$$\nu_\alpha = \sqrt{\left(\nu_I - \frac{A}{2}\right)^2 + \left(\frac{B}{2}\right)^2};\nu_\beta = \sqrt{\left(\nu_I + \frac{A}{2}\right)^2 + \left(\frac{B}{2}\right)^2} \quad (3)$$

The Cu(II)−Aβ_{1-16} complexes show little orientation selectivity in the ESEEM spectrum at $g_\perp$ for the Cu(II), and the Cu(II)-coordinating histidine is perpendicular to the $g_\parallel$ axis (*26, 28*). Therefore, an axial hyperfine tensor is assumed for this system, and the two frequencies, ν_α and ν_β, are related by the equation (*47*−*50*)

$$\nu_\alpha = Q\nu_\beta + G \quad (4)$$

where

$$Q = \frac{T + 2A_{iso} - 4\nu_I}{T + 2A_{iso} + 4\nu_I} \quad (5)$$

$$G = 2\nu_I \frac{4\nu_I - A_{iso} + 2T^2 - A_{iso}T}{T + 2A_{iso} + 4\nu_I} \quad (6)$$

A_{iso} and T are the isotropic component and the anisotropic component of the hyperfine constant, respectively. Equation 4 accounts for the line shape of the ^{15}N cross-peak in the contour plot (Figure 6): it is an elliptic or hyperbolic arc. The HYSCORE spectra of Cu(II)−Aβ_{1-16}H6[^{15}N], Cu(II)−Aβ_{1-16}H13[^{15}N], and Cu(II)−Aβ_{1-16}H14[^{15}N] complexes, shown as spectra b−d of Figure 6, respectively, have similar ^{15}N cross-peak positions and contour line shapes, which indicates that the hyperfine coupling parameters for the three histidine residues are nearly identical. The Cu(II)−His13 and Cu(II)−His14 hyperfine couplings may be different because His13 and His14 are adjacent residues; therefore, the two residues are unlikely to attain similar binding conformations. Nevertheless, we were unable to detect substantial differences possibly due to the resolution of the data set. Such differences can be more quantitatively measured by the use of doubly ^{15}N-labeled peptide analogues. The two constants, Q and G, are determined to be −0.154 and 1.23 MHz^2, respectively, by plotting ν_α^2 versus ν_β^2, and A_{iso} and $|T|$ for ^{15}N are calculated to be 2.33 and 0.413 MHz, respectively. The parameters strongly suggest that the binding affinity of the Cu(II)−histidine coupling in Aβ_{1-16} is high because the hyperfine coupling constants are greater than those for Cu(II) complexes of imidazole derivatives that were studied by McCracken et al. (*27, 28*). The strong hyperfine interaction may explain the submicromolar-level dissociation constant of the Cu(II)−Aβ peptide complex reported by Syme et al. (*17*).

SUMMARY

In this article, we elucidate the binding of Cu(II) to the three histidine residues in the Aβ_{1-16} peptide with no amino acid side chain modification or replacement of residue(s). Employing ESEEM and HYSCORE techniques with the nonlabeled Aβ_{1-16} peptide and ^{15}N-labeled analogues, we reveal that ^{15}N labeling of each histidine leads to a significant change in the ESR spectra. The ESEEM spectra of the singly ^{15}N-labeled analogues exhibit lower intensities when compared with the nonlabeled Aβ_{1-16} peptide. In addition, direct evidence of a strong hyperfine interaction between the Cu(II) ion and each histidine residue is obtained from the HYSCORE spectra. Our data also illustrate that the Cu(II)-binding site in Aβ_{1-16} is not sensitive to the Cu(II)-to-peptide ratio, which is in contrast to the case of the Aβ_{1-40} peptide.

ACKNOWLEDGMENT

We are grateful to Sangmi Jun and Dr. Sharon Ruthstein for helpful discussions. We also thank the Peptide Synthesis Facility of the University of Pittsburgh for the peptide preparation.

REFERENCES

1. McLaurin, J., and Chakrabartty, A. (1996) Membrane Disruption by Alzheimer β-Amyloid Peptides Mediated through Specific Binding to either Phospholipids or Gangliosides: Implications for Neurotoxicity. *J. Biol. Chem. 271*, 26482–26489.
2. Walsh, D. M., Lomakin, A., Benedek, G. B., Condron, M. M., and Teplow, D. B. (1997) Amyloid β-Protein Fibrillogenesis. Detection of a Protofibrillar Intermediate. *J. Biol. Chem. 272*, 22364–22372.
3. Lambert, M. P., Barlow, A. K., Chromy, B. A., Edwards, C., Freed, R., Liosatos, M., Morgan, T. E., Rozovsky, I., Trommer, B., Viola, K. L., Wals, P., Zhang, C., Finch, C. E., Krafft, G. A., and Klein, W. L. (1998) Diffusible, Nonfibrillar Ligands Derived from Aβ_{1-42} are Potent Central Nervous System Neurotoxins. *Proc. Natl. Acad. Sci. U.S.A. 95*, 6448–6453.
4. Hardy, J., and Selkoe, D. J. (2002) The Amyloid Hypothesis of Alzheimer's Disease: Progress and Problems on the Road to Therapeutics. *Science 297*, 353–356.
5. Carrotta, R., Manno, M., Bulone, D., Martorana, V., and San Biagio, P. L. (2005) Protofibril Formation of Amyloid β-Protein at Low pH via a Non-cooperative Elongation Mechanism. *J. Biol. Chem. 280*, 30001–30008.
6. Lovell, M. A., Robertson, J. D., Teesdale, W. J., Campbell, J. L., and Markesbery, W. R. (1998) Copper, Iron and Zinc in Alzheimer's Disease Senile Plaques. *J. Neurol. Sci. 158*, 47–52.
7. Huang, X., Cuajungco, M., Atwood, C. G., Hartshorn, M. A., Tyndall, J. D. A., Hanson, G. R., Stokes, K. C., Leopold, M., Multhaup, G., Goldstein, L. E., Scarpa, R. C., Saunders, A. J., Lom, J., Moir, R. D., Glabe, C., Bowden, E. F., Masters, C. L., Fairlie, D. P., Tanzi, R. E., and Bush, A. I. (1999) Cu(II) Potentiation of Alzheimer Aβ Neurotoxicity. *J. Biol. Chem. 274*, 37111–37116.
8. Bush, A. I. (2002) Metal Complexing Agents and Therapies for Alzheimer's Disease. *Neurobiol. Aging 23*, 1031–1038.
9. Kirkitadze, M. D., Bitan, G., and Teplow, D. B. (2002) Paradigm Shifts in Alzheimer's Disease and Other Neurodegenerative Disorders: The Emerging Role of Oligomeric Assemblies. *J. Neurosci. Res. 69*, 567–577.
10. Miller, L. M., Wang, Q., Telivala, T. P., Smith, R. J., Lanzirotti, A., and Miklossy, J. (2006) Synchrotron-Based Infrared and X-ray Imaging Shows Focalized Accumulation of Cu and Zn Co-Localized with β-Amyloid Deposits in Alzheimer's Disease. *J. Struct. Biol. 155*, 30–37.
11. (a) Jun, S., and Saxena, S. (2007) The Aggregated State of Amyloid-β Peptide in vitro Depends on Cu^{2+} Ion Concentration. *Angew. Chem., Int. Ed. 46*, 3959–3961. (b) Jun, S., and Saxena, S. (2007) The Aggregated State of Amyloid-β Peptide in vitro Depends on Cu^{2+} Ion Concentration. *Angew. Chem., Int. Ed. 46*, 5263.
12. Karr, J. W., Kaupp, L. J., and Szalai, V. A. (2004) Amyloid-β Binds Cu^{2+} in a Mononuclear Metal Ion Binding Site. *J. Am. Chem. Soc. 126*, 13534–13538.
13. Karr, J. W., Akintoye, H., Kaupp, L. J., and Szalai, V. A. (2005) N-Terminal Deletions Modify the Cu^{2+} Binding Site in Amyloid-β. *Biochemistry 44*, 5478–5487.
14. Karr, J. W., and Szalai, V. A. (2008) Cu(II) Binding to Monomeric, Oligomeric, and Fibrillar Forms of the Alzheimer's Disease Amyloid-β Peptide. *Biochemistry 47*, 5006–5016.
15. Peisach, J., and Blumberg, W. E. (1974) Structural Implications Derived from the Analysis of Electron Paramagnetic Resonance Spectra of Natural and Artificial Copper Proteins. *Arch. Biochem. Biophys. 165*, 691–708.
16. Kowalik-Jankowska, T., Ruta, M., Wisniewska, K., and Lankiewicz, L. (2003) Coordination Abilities of the 1−16 and 1−28 Fragments of β-Amyloid Peptide towards Copper(II) Ions: A Combined Potentiometric and Spectroscopic Study. *J. Inorg. Biochem. 95*, 270–282.
17. Syme, C. D., Nadal, R. C., Rigby, S. E. J., and Viles, J. H. (2004) Copper Binding to the Amyloid-β (Aβ) Peptide Associated with Alzheimer's Disease: Folding, Coordination Geometry, pH Dependence, Stoichiometry, and Affinity of Aβ-(1−28): Insights from a Range of Complementary Spectroscopic Techniques. *J. Biol. Chem. 279*, 18169–18177.
18. Raffa, D. F., and Rauk, A. (2007) Molecular Dynamics Study of the β Amyloid Peptide of Alzheimer's Disease and Its Divalent Copper Complexes. *J. Phys. Chem. B 111*, 3789–3799.
19. Aronoff-Spencer, E., Burns, C. S., Avedievich, N. I., Gerfen, G. J., Peisach, J., Antholine, W. E., Ball, H. L., Cohen, F. E., Prusiner, S. B., and Millhauser, G. L. (2000) Identification of Cu^{2+} Binding Sites in the N-Terminal Domain of the Prion Protein by EPR and CD Spectroscopy. *Biochemistry 39*, 13760–13771.
20. Burns, C. S., Aronoff-Spencer, E., Dunham, C. M., Lario, P., Avedievich, N. I., Antholine, W. E., Olmstead, M. M., Vrielink,

A., Gerfen, G. J., Peisach, J., Scott, W. G., and Millhauser, G. L. (2002) Molecular Features of the Copper Binding Sites in the Octarepeat Domain of the Prion Protein. *Biochemistry 41*, 3991–4001.
21. Burns, C. S., Aronoff-Spencer, E., Legname, G., Prusiner, S. B., Antholine, W. E., Gerfen, G. J., Peisach, J., and Millhauser, G. L. (2003) Copper Coordination in the Full-Length, Recombinant Prion Protein. *Biochemistry 42*, 6794–6803.
22. Atwood, C. S., Scarpa, R. C., Huang, X., Moir, R. D., Jones, W. D., Fairlie, D. P., Tanzi, R. E., and Bush, A. I. (2000) Characterization of Copper Interactions with Alzheimer Amyloid β Peptides: Identification of an Attomolar-Affinity Copper Binding Site on Amyloid β1−42. *J. Neurochem. 75*, 1219–1233.
23. Fauth, J.-M., Schweiger, A., Braunschweiler, A., Forrer, J., and Ernst, R. R. (1986) Elimination of Unwanted Echoes and Reduction of Dead Time in Three-Pulse Electron Spin-Echo Spectroscopy. *J. Magn. Reson. 66*, 74–85.
24. Gemperle, C., Aebli, G., Schweiger, A., and Ernst, R. R. (1990) Phase Cycling in Pulse EPR. *J. Magn. Reson. 88*, 241–256.
25. Dikanov, S. A., Tsvetkov, Y. D., Bowman, M. K., and Astashkin, A. V. (1982) Parameters of Quadrupole Coupling of ^{14}N Nuclei in Chlorophyll a Cations Determined by the Electron Spin Echo Method. *Chem. Phys. Lett. 90*, 149–153.
26. McCracken, J., Peisach, J., and Dooley, D. M. (1987) Cu(II) Coordination Chemistry of Amine Oxidase: Pulsed EPR Studies of Histidine Imidazole, Water, and Exogenous Ligand Coordination. *J. Am. Chem. Soc. 109*, 4064–4072.
27. McCracken, J., Pember, S., Benkovic, S. J., Villafranca, J. J., Miller, R. J., and Peisach, J. (1988) Electron Spin-Echo Studies of the Copper Binding Site in Phenylalanine Hydroxylase from *Chromobacterium violaceum*. *J. Am. Chem. Soc. 110*, 1069–1074.
28. Jiang, F., McCracken, J., and Peisach, J. (1990) Nuclear Quadrupolar Interactions in Cu(II)-Diethylenetriamine-Substituted Imidazole Complexes and Cu(II) Proteins. *J. Am. Chem. Soc. 112*, 9035–9044.
29. Flanagan, H. L., and Singel, D. J. (1987) Analysis of ^{14}N ESEEM Patterns of Randomly Oriented Solids. *J. Chem. Phys. 87*, 5606–5616.
30. Mims, W. B. (1972) Envelope Modulation in Spin-Echo Experiments. *Phys. Rev. B 5*, 2409–2419.
31. Kosman, D. J., Peisach, J., and Mims, W. B. (1980) Pulsed Electron Paramagnetic Resonance Studies of the Cu(II) Site in Galactose Oxidase. *Biochemistry 19*, 1304–1308.
32. Astashkin, A. V., and Kawamori, A. (1995) A New Fourier-Transformation-Based Algorithm for Data Filtering and Extrapolation. *J. Magn. Reson., Ser. A 112*, 24–29.
33. Kevan, L., Bowman, M. K., Narayana, P. A., Boeckman, R. K., Yudanov, V. F., and Tsvetkov, Y. D. (1975) Electron Spin Echo Envelope Modulation of Trapped Radicals in Disordered Glassy Systems: Application to the Molecular Structure around Excess Electron in γ-irradiated 2-Methyltetrahydrofuran Glass. *J. Chem. Phys. 63*, 409–416.
34. Mims, W. B., and Davis, J. L. (1976) Proton Modulation of the Electron Spin Echo Envelope in an Nd^{3+}: Aquo Glass. *J. Chem. Phys. 64*, 4836–4846.
35. Vogt, M., Lahiri, S., Hoogstraten, C. G., Britt, R. D., and DeRose, V. J. (2006) Coordination Environment of a Site-Bound Metal Ion in the Hammerhead Ribozyme Determined by ^{15}N and ^{2}H ESEEM Spectroscopy. *J. Am. Chem. Soc. 128*, 16764–16770.
36. Lai, A., Flanagan, H. L., and Singel, D. J. (1988) Multifrequency Electron Spin Echo Envelope Modulation in S=1/2, I=1/2 Systems: Analysis of the Spectral Amplitudes, Line Shapes, and Linewidths. *J. Chem. Phys. 89*, 7161–7166.
37. McCracken, J., Peisach, J., Cote, C. E., McGuirl, M. A., and Dooley, D. M. (1992) Pulsed EPR Studies of the Semiquinone State of Copper-Containing Amine Oxidases. *J. Am. Chem. Soc. 114*, 3715–3720.
38. Tang, X.-S., Diner, B. A., Larsen, B. S., Gilchrist, M. L., Lorigan, G. A., and Britt, R. D. (1994) Identification of Histidine at the Catalytic Site of the Photosynthetic Oxygen-Evolving Complex. *Proc. Natl. Acad. Sci. U.S.A. 91*, 704–708.
39. Singh, V., Zhu, Z., Davidson, V. L., and McCracken, J. (2000) Characterization of the Tryptophan Tryptophyl-Semiquinone Catalytic Intermediate of Methylamine Dehydrogenase by Electron Spin-Echo Envelope Modulation Spectroscopy. *J. Am. Chem. Soc. 122*, 931–938.
40. Hofer, P., Grupp, A., Nebenfuhr, H., and Mehring, M. (1986) Hyperfine Sublevel Correlation (HYSCORE) Spectroscopy: A 2D ESR Investigation of the Squaric Acid Radical. *Chem. Phys. Lett. 132*, 279–282.
41. Goldfarb, D., Fauth, J.-M., Tor, Y., and Shanzer, A. (1991) Study of Cu(II) Binding to Chiral Tripodal Ligands by Electron Spin Echo Spectroscopy. *J. Am. Chem. Soc. 113*, 1941–1948.
42. Poppl, A., and Kevan, L. (1996) A Practical Strategy for Determination of Proton Hyperfine Interaction Parameters in Paramagnetic Transition Metal Ion Complexes by Two-Dimensional HYSCORE Electron Spin Resonance Spectroscopy in Disordered Systems. *J. Phys. Chem. 100*, 3387–3394.
43. Ponti, A., and Schweiger, A. (1995) Nuclear Coherence-Transfer Echoes in Pulsed EPR. *J. Chem. Phys. 102*, 5207–5219.
44. Kofman, V., Shane, J. J., Dikanov, S. A., Bowman, M. K., Libman, J., Shanzer, A., and Goldfarb, D. (1995) Coordination of Cu(II) to Lipophilic Bis-hydroxamate Binders As Studied by One- and Two-Dimensional Electron Spin Echo Spectroscopy. *J. Am. Chem. Soc. 117*, 12771–12778.
45. Kofman, V., Farver, O., Pecht, I., and Goldfarb, D. (1996) Two-Dimensional Pulsed EPR Spectroscopy of the Copper Protein Azurin. *J. Am. Chem. Soc. 118*, 1201–1206.
46. Mims, W. B., and Peisach, J. (1978) The Nuclear Modulation Effect in Electron Spin Echoes for Complexes of Cu^{2+} and Imidazole with ^{14}N and ^{15}N. *J. Chem. Phys. 69*, 4921–4930.
47. Dikanov, S. A., and Bowman, M. K. (1995) Cross-Peak Lineshape of Two-Dimensional ESEEM Spectra in Disordered S=1/2, I=1/2 Spin Systems. *J. Magn. Reson., Ser. A 116*, 125–128.
48. Dikanov, S. A., Tyryshkin, A. M., and Bowman, M. K. (2000) Intensity of Cross-Peaks in Hyscore Spectra of S=1/2, I=1/2 Spin Systems. *J. Magn. Reson. 144*, 228–242.
49. Hofer, P. (1994) Distortion-Free Electron-Spin-Echo Envelope-Modulation Spectra of Disordered Solids Obtained from Two-Dimensional and Three-Dimensional HYSCORE Experiments. *J. Magn. Reson., Ser. A 111*, 77–86.
50. Kass, H., Rautter, J., Bonigk, B., Hofer, P., and Lubitz, W. (1995) 2D ESEEM of the ^{15}N-Labeled Radical Cations of Bacteriochlorophyll α and of the Primary Donor in Reaction Centers of Rhodobacter sphaeroides. *J. Phys. Chem. 99*, 436–448.

BI801014X